Chemical Engineering Science 142 (2016) 180–189

Contents lists available at ScienceDirect

Chemical Engineering Science

journal homepage: www.elsevier.com/locate/ces

Block length determines the adsorption dynamics mode of triblock copolymers to a hydrophobic surface

Yisheng Xu [a,b], Kaihang Shi [b], Shuangliang Zhao [a,b,*], Xuhong Guo [a,b], Jie Wang [a,b,*]

[a] State Key Laboratory of Chemical Engineering, East China University of Science and Technology, Shanghai 200237, China
[b] Shanghai Key Laboratory of Multiphase Materials Chemical Engineering, East China University of Science and Technology, Shanghai 200237, China

HIGHLIGHTS

- Polymer block length determines the adsorption dynamics to liquid/solid interface.
- Above CMC P100 polymers present three-stage adsorption and form two-layer structure.
- P500 polymers display monotonous adsorption and form uniform adsorbed structure.
- The adsorption mechanism is explored with DPD simulation from molecular interaction.

ARTICLE INFO

Article history:
Received 30 June 2015
Received in revised form
15 November 2015
Accepted 29 November 2015
Available online 14 December 2015

Keywords:
Adsorption dynamics
Block copolymer
Hydrophobic surface
Block-length effect

ABSTRACT

Many material processes including surface modification and material fabrication depend on the mechanism by which polymers are adsorbed onto solid/liquid interfaces. Although the morphologies of block copolymers near the interface have been extensively investigated, the understanding of the adsorption dynamics is still limited. Here, we show that the block length determines the dynamic adsorption mode under conditions beyond the critical micelle concentration (CMC). The adsorption kinetics are investigated using in situ experimental characterization combined with Dissipative Particle Dynamics simulations. Two types of symmetrical triblock copolymers, i.e., PEO–PPO–PEO, with different hydrophilic PEO block lengths are studied. While both types of copolymers present similar adsorption dynamics at concentrations below the CMC, their dynamic adsorption modes are distinct at concentrations above the CMC. The present experimental–numerical study provides a mechanistic interpretation of this difference, which casts helpful insight for the dynamic control process of surface modification and material fabrication.

1. Introduction

The adsorption of polymers at solid/liquid interfaces has received increasing attentions due to their importance in the stabilization of colloids, development of materials, surface modification, and advancements in life science (Napper, 1983; Chakraborty and Golumbfskie, 2001; Frisch et al., 1953; Silberberg, 1962; Scheutjens and Fleer, 1979; Watts et al., 1984; Munch and Gast, 1988; Zhu and Gu, 1991; Wang and Mattice, 1994; Zhan and Mattice, 1994; Amiel et al., 1995; Misra, 1996; Huang et al., 2002). In comparison with homopolymers, block copolymers usually exhibit specific adsorption behavior, forming a variety of structures such as micelles or lamellae in appropriate solvents (Frisch et al., 1953; Munch and Gast, 1988; Wang and Mattice, 1994; Amiel et al., 1995). For instance, Brandani and Stroeve (2003) investigated the adsorption from water of a family of triblock poly (ethylene oxide)-b-poly(propylene oxide)-b-poly(ethylene oxide) copolymers, i.e., $(PEO)_n$–$(PPO)_m$–$(PEO)_n$ (the subscripts n and m represent the number of repeat units), on a hydrophobic surface and observed that the morphology adopted by the triblock copolymers on the surface was closely associated with the composition of the blocks. Li et al. (2011) studied the adsorption of $(PEO)_{19}$–$(PPO)_{29}$–$(PEO)_{19}$ on three different substrates using Atomic Force Microscopy, and significant morphological differences were found. In addition to the chemical composition and surface properties, the effects of concentration and temperature on the adsorption of block copolymers in equilibrium have also been investigated (Brandani and Stroeve, 2003; Kamerlin et al., 2011; Marques et al.,

* Corresponding authors.
E-mail addresses: szhao@ecust.edu.cn (S. Zhao), jiewang2010@ecust.edu.cn (J. Wang).

http://dx.doi.org/10.1016/j.ces.2015.11.045
0009-2509/

1988; Johner and Joanny, 1990; Munch and Gast, 1990; Tiberg et al., 1991; Alexandridis et al., 1994; Eskilsson and Tiberg, 1997; Green et al., 1997; Emoto et al., 1999).

However, the majority of work previously reported focuses on the equilibrium properties of adsorbed polymers, including the morphology of the polymer on different substrates, the physicochemical and thermodynamic properties of the adsorbed polymers (Chen et al., 2003, 2001; Guo et al., 2003) or tethered polymer brushes (Tong, 2014; Lian et al., 2014a, 2014b), and investigations concerning the adsorption dynamics of polymers from a solvent onto a substrate are still limited (Munch and Gast, 1988; Johner and Joanny, 1990; Munch and Gast, 1990; Eskilsson and Tiberg, 1997). Generally, polymeric micelles are not expected to be adsorbed directly onto a solid surface. Instead, they act as reservoirs for chains to be adsorbed (Munch and Gast, 1988; Johner and Joanny, 1990). The adsorption process is believed to consist of several stages. First, free chains cover the unoccupied surface through diffusion. Second, due to the aggregation and disaggregation equilibrium between micelles and free polymer chains in solution, some polymer chains are released from the micelles and are then adsorbed onto the surface. In this stage, the adsorption dynamics are dominated by the chain expulsion from the micelles. Third, due to the exclusion of the pre-adsorbed chains to incoming chains, the adsorption process slows down. Finally, the surface is saturated with polymer chains and the adsorption terminates (Munch and Gast, 1988; Johner and Joanny, 1990). Empirically it has been observed that poly(ethylene oxide)-b-poly(tetrahydrofuran)-b-poly(ethylene oxide) exhibits a three-regime adsorption onto a water/hydrophobic silica interface, involving a diffusion-controlled regime, substitution-limited regime, and brush-dominated regime (Eskilsson and Tiberg, 1997). On the other hand, Munch and Gast (1990) demonstrated that polystyrene-b-poly(ethylene oxide) exhibited a much faster adsorption at concentrations above the critical micelle concentration (CMC) than below the CMC. It has also been shown that the amount of PEO–PPO–PEO adsorbed onto a hydrophobic surface significantly increases at concentrations above the CMC due to the formation of a multilayer structure (Tiberg et al., 1991). Nevertheless, the adsorption mechanism of block copolymers is not well understood, particularly the adsorption dynamics.

In the present study, we investigate the adsorption of PEO–PPO–PEO triblock copolymers with different hydrophilic PEO block lengths from an aqueous solution to a hydrophobic surface in situ using a quartz crystal microbalance with dissipation (QCM-D) and Surface Plasmon Resonance (SPR). Further theoretical investigations are performed using Dissipative Particle Dynamics (DPD) simulations, which provide a more detailed and tangible depiction of the adsorption dynamics. The effect of the PEO block length on the adsorption dynamics, in particular, is addressed.

2. Experimental section

2.1. Materials

Two kinds of PEO–PPO–PEO samples, i.e., $(PEO)_4$–$(PPO)_{56}$–$(PEO)_4$ and $(PEO)_{37}$–$(PPO)_{56}$–$(PEO)_{37}$, are considered. These triblock copolymers have the same PPO block length but different PEO block lengths, are hereafter referred as P100 (with short PEO block length) and P500 (with long PEO block length). BASF® (BASF, China) donated these samples, and for P100, M_w=3610 g/mol, 10 wt% PEO, and for P500, M_w=6500 g/mol, 50 wt% PEO. Undecanethiol and ethanol (SINOPHARM® SINOPHARM, China) were used as received.

2.2. Preparation of the hydrophobic surface

The representative hydrophobic surface used in this study is an undecanethiol-modified gold surface (Creager and Clarke, 1994). QCM-D and SPR gold sensor chips were first cleaned using Piranha solution (H_2SO_4/H_2O_2, V/V=3:1), rinsed with deionized water, and then dried under a nitrogen flow. The self-assembly of each hydrophobic monolayer was achieved by immersing the freshly cleaned chips in a 5.0 mM undecanethiol solution in ethanol for 20 h (Creager and Clarke, 1994). The QCM-D crystal was mounted in a protective casing made of Teflon to shield the other side from the undecanethiol solution. The SPR sensor chip was immersed directly into the undecanethiol solution. The modified chips were rinsed with adequate alcohol and water to remove residual undecanethiol before being dried under a nitrogen flow.

2.3. Laser Light Scattering (LLS)

Laser Light Scattering (LLS) measurements were conducted on an ALV/DLS/SLS-5022F spectrometer equipped with a multi τ digital time correlation (ALV5000, ALV® Langen (Germany)) and a cylindrical 22 mW UNIPHASE He–Ne laser (λ_0=632 nm) light source. The CMC of each PEO–PPO–PEO solution was determined by dynamic LLS because the scattered light intensity was sensitive to polymer aggregation. The solution was filtered using a 0.45-μm Millipore filter to remove dust before the measurements. All LLS measurements were performed at 25 °C and at a scattering angle of 90°. The CMC for P100 and P500 were determined as 0.1 and 0.59 mg/mL, respectively.

2.4. QCM-D measurements

The QCM-D and the AT-cut quartz crystal with a fundamental resonant frequency of 5 MHz were from Q-sense AB (Rodahl et al., 1995). The measurable frequency shift is within ± 1 Hz in aqueous media. The effects of surface roughness are neglected because the crystal is highly polished with a root-mean-square roughness less than 3 nm (Chen et al., 2001).

When a quartz crystal is excited to oscillate in the thickness shear mode at its fundamental resonant frequency by applying a RF voltage across the electrodes, a small change in the mass added on the electrodes results in a decrease in the resonant frequency (Δf). In vacuum or air, if the added layer is rigid, evenly distributed, and much thinner than the crystal, Δf is related to Δm (the mass change of the added layer per area) and the overtone number (n=1, 3, 5….) through the Sauerbrey equation (Sauerbrey, 1959):

$$\Delta m = -\frac{\rho_q l_q}{f_0}\frac{\Delta f}{n} = -K\frac{\Delta f}{n} \quad (1)$$

where f_0 is the fundamental frequency, and ρ_q and l_q are the specific density and thickness of the quartz crystal, respectively. The constant (K) of the AT-cut quartz crystal is 17.7 ng/cm^2 Hz (Rodahl et al., 1995; Zheng et al., 2014) The dissipation factor (ΔD) is defined by $\Delta D = E_d/2\pi E_s$, where E_d is the energy dissipated during one oscillation and E_s is the energy stored in the oscillating system. The measurement of ΔD is based on the fact that the voltage over the crystal decays exponentially as a damped sinusoidal when the driving power of a piezoelectric oscillator is switched off (Rodahl et al., 1995). By switching the driving voltage on and off periodically, we can simultaneously obtain a series of changes in the resonant frequency and the dissipation factor.

The solvent effect on the frequency and dissipation responses could be removed by using the corresponding solvent as the reference (Stockbridge, 1966; Kanazawa and Gordon, 1985; Rodahl and Kasemo, 1996). Both Δf and ΔD values were recorded in the

ninth overtone ($n=3$), discarding the fundamental and higher overtones due to insufficient energy trapping or weak reproducibility (Lucklum and Hauptmann, 2003). All experiments were performed at 25.0 ± 0.02 °C.

2.5. SPR measurements

SPR experiments were conducted with a BIAcore™ X (BIAcore, Sweden) with Au sensor chips at 25 °C (Sjolander and Urbaniczky, 1991). In Krestchmann mode, when the wave vector of the surface plasmon and the vector of the incident light along the metal surface match at a certain incidence angle, the light energy is coupled with the surface plasmon, leading to a sharp minimum in the reflectivity curve. The incident angle there is called the SPR angle (Pockrand, 1978; Knoll, 1998). The change in the reflective index in the vicinity of the surface induces a shift in the SPR angle that is proportional to the change in the resonance unit (RU), i.e., ΔR. Here, 1000 RU is equivalent to a SPR angle change of 1°. The polymer solution was applied to the sensor surface at a flow rate of 10 μL/min.

3. Modeling and simulation

3.1. Model and method

To probe the adsorption kinetics at molecular level, Dissipative Particle Dynamics (DPD) simulations are performed. DPD is a coarse-grained simulation method basing on simplified Hamiltonians with solvent being treated as continuum and a certain number of solute molecules being grouped into a DPD bead (Groot and Warren, 1997), and in addition, unlike conventional molecular dynamics simulation in which the choice of pairwise additive interaction is based on a theoretical model of the physical system to be simulated, DPD method involves the potential of a form independent of the physical system (Keaveny et al., 2005). For these reasons, DPD simulation has been becoming a useful tool allowing for the description of mesoscopic phenomena (Groot and Warren, 1997; Feng et al., 2007; Feng et al., 2006; Hoogerbrugge and Koelman, 1992; Espanol and Warren, 1995). The system under investigation is composed of water and triblock copolymers. The principle of building a coarse-grained model for triblock copolymers is the same as in Ref. Chen et al. (2007). Four PEO or three PPO segments are grouped into one DPD bead, denoted as EO (E) or PO (P) bead, and this coarse-grained mapping method ensures that both the EO and PO beads have a comparable size of 240 Å^3 (Groot and Rabone, 2001). Because water molecule has a volume of 30 Å^3 (Groot and Rabone, 2001), in order to have the same size as both EO and PO beads eight water molecules are grouped into one DPD water bead (W). The bead density of the whole system is $\rho {r_c}^3 = 3$, and this means there are three DPD beads within a cubic of ${r_c}^3$. Accordingly, the physical size of the interaction radius involved in the bead-bead interactions (see below) can be determined as

$$r_c = \sqrt[3]{3 \times 240}\ \text{Å} = 8.96\ \text{Å} \tag{2}$$

The coarse-grained models for P100 and P500 are represented by the linear chains of $(EO)_1(PO)_{18}(EO)_1$ and $(EO)_9(PO)_{18}(EO)_9$, respectively. Note that both models do not rigorously correspond to P100 and to P500, respectively, and very small deviations on segment numbers exist. However, those differences should be negligible.

The modified gold surface used experimentally is modeled as an implicit hydrophobic surface in our simulation. The implicit description of a solid surface is commonly used in both atomistic methods (Bandyopadhyay et al., 1998; Lee and Rossky, 1994) and coarse-grained approaches (Srinivas et al., 2006). In our model system, two symmetric hydrophobic surfaces are placed in parallel separated by a distance d. It should be noted that the distance between these two surfaces must be sufficiently large to ensure the surface potential decays to zero in the middle but also to create a large enough space for micelle formation (Srinivas et al., 2006). For these reasons, we set $d = 20r_c$ here, which is large enough for the triblock copolymers to form micelles as observed in our simulation.

The particle positions and velocities are governed by Newton's laws of motion:

$$\begin{cases} \frac{d\mathbf{r}_i}{dt} = \mathbf{v}_i \\ m_i \frac{d\mathbf{v}_i}{dt} = \mathbf{F}_i \end{cases} \tag{3}$$

where $\mathbf{r}_i$, $\mathbf{v}_i$ and m_i are the position, velocity and mass of the ith bead, respectively. $\mathbf{F}_i$ is the total force exerted on bead i. The total force is composed of three parts, each of which is pair-wise additive,

$$\mathbf{F}_i = \sum_{j=1, j\neq i}^{N} (\mathbf{F}_{ij}^{C} + \mathbf{F}_{ij}^{D} + \mathbf{F}_{ij}^{R}) \tag{4}$$

Here, $\mathbf{F}_{ij}^{C}$ is the conservative force, and $\mathbf{F}_{ij}^{D}$ and $\mathbf{F}_{ij}^{R}$ are the dissipative force and random force, respectively. The conservative force between bead i and j is given by

$$\mathbf{F}_{ij}^{C} = \begin{cases} a_{ij}(1 - r_{ij}/r_c)\hat{\mathbf{r}}_{ij} & (r_{ij} < r_c) \\ 0 & (r_{ij} \geq r_c) \end{cases} \tag{5}$$

where $r_{ij} = r_i - r_j$ is the distance between the ith and the jth beads. The unit vector, $\hat{\mathbf{r}}_{ij}$, denotes the direction from bead i to j. r_c represents the interaction range. The coefficient, a_{ij}, represents the maximum repulsion between the ith and the jth beads, and it can be calculated from the Flory–Huggins binary interaction parameter, χ_{ij}, using the relation below for $\rho {r_c}^3 = 3$ as discussed in Ref. Shi et al. (2014),

$$a_{ij} = (a_{ii} + 3.27\chi_{ij})\frac{k_B T}{r_c} \tag{6}$$

Here, k_B is the Boltzmann constant, and T is the absolute temperature. Throughout our simulation, reduced DPD units are used. Specifically, r_c is taken as the length unit. $k_B T$ is the unit of energy. The mass of each beads m is set equal. Thus the unit of time step τ can be calculated by

$$\tau = r_c \sqrt{\frac{m}{k_B T}} \tag{7}$$

In the present work the time unit $\tau = 7.32$ ps for an average mass $m = 2.741 \times 10^{-25}$ kg.

3.2. Parameters and computational details

The interaction parameters (a_{ij}) in Eq. (6) are similar to that of Ref. Chen et al. (2007) in which the adsorption of PEI–PPO–PEO block copolymers onto the surface of gold nanoparticles was simulated using the DPD method. The interaction parameters employed in this work are given in Table 1. Note that the parameter a_{ij} between the EO segment and water has changed from

Table 1
Conservative interaction parameters a_{ij} in units of $k_B T/r_c$. Here, E, P, and W represent the EO bead, PO bead and water bead, respectively.

	E	P	W	Hydrophobic surface
E	25	48.87	25	60
P	48.87	25	38.32	25
W	25	38.32	25	36

35.93 to 25 to mimic the strong affinity between these two components. The QCM-D and SPR gold sensor chips used in this study were treated with Piranha solution. This treatment enhanced the hydrophilicity of the surface to some extent, even though the surface was covered by a hydrophobic monolayer and rinsed and dried afterwards. For this reason, the interaction parameters between the hydrophobic surface and coarse-grained beads were reset in this study, differing slightly from those used in Ref. Chen et al. (2007). The successful reproduction of experimental results, as shown in the latter, indicates the applicability of the interaction parameters used.

The simulation box was set to $40 \times 40 \times 20 r_c^3$ ($L_x \times L_y \times L_z$), with periodic boundary conditions applied in x- and y-directions. The numbers of P100 and P500 copolymers in the simulation box are fixed. Initial configurations were generated by inserting coarse-grained copolymers and water beads randomly into the simulation cell.

The DPD simulations were performed with the help of a DPD module in *Material Studio* 6 (Accelrys, Materials Studio). A total of 400,000 time steps were carried out to equilibrate the system, and the diffusivity of each component in the system became nearly constant after 300,000 time steps. As tested by Groot and Warren (1997) the choice of time step is a trade-off between the relaxation time and the thermos-stability, and it could vary from 0.001τ to 0.06τ without significant loss of temperature control. Here we take the time step as 0.05τ.

4. Results and discussion

4.1. Adsorption dynamics of P500 and P100

Fig. 1 plots the changes in frequency (Δf) and dissipation (ΔD) of the quartz resonator during the adsorption and desorption of P500 and P100 onto/from the undecanethiol-modified gold surface. The adsorption dynamics of P500 are illustrated in Fig. 1a and b, and those for P100 are shown in Fig. 1a′ and b′. In both cases, three polymeric concentrations are considered, i.e., 0.5 CMC, 2.0 CMC and 3.0 CMC. As discussed above, Δf reflects the mass change of the adsorbed layer, and ΔD is related to its thickness and compactness. The curves record these changes in three periods: dynamic adsorption, equilibrium and rinsing.

Generally, curves of Δf and ΔD are concentration-dependent. When the concentration of the copolymers (regardless of P500 or P100) is higher, the equilibrium value (and residue value) of ΔD is higher, while Δf is lower. This is understandable because the higher osmotic pressure at higher concentrations leads to more chains being adsorbed onto the surface. By using computer simulations, Liu and coworkers (Sun et al., 2007; Peng et al., 2005) demonstrated that the thickness of adsorbed polymers depends on the chain lengths, block length, bulk concentration, and the adsorption energy between the substrate and polymers. In particular, they predicted that when the adsorption energy was large, the thickness increased as a logarithm function of the bulk polymer concentration (Sun et al., 2007). The variation in ΔD with concentration is displayed in Fig. 1 and generally confirms their predictions. Rinsing with water leads to an increase in Δf and a decrease in ΔD in all systems. This is because the polymer solution is replaced by water and then the adsorbed polymer is partially washed away from the surface. Therefore, the density and viscoelasticity near the surface decrease.

The adsorption dynamics are the major interest of the present work. We will first discuss the adsorption dynamics of P500. As observed, when the solvent (water) is replaced by a polymer solution, initially, a significant decrease in Δf and an increase in ΔD are observed. Both of these changes indicate a fast adsorption of P500 from solution onto the surface. However, after the fast adsorption, the frequency and dissipation do not

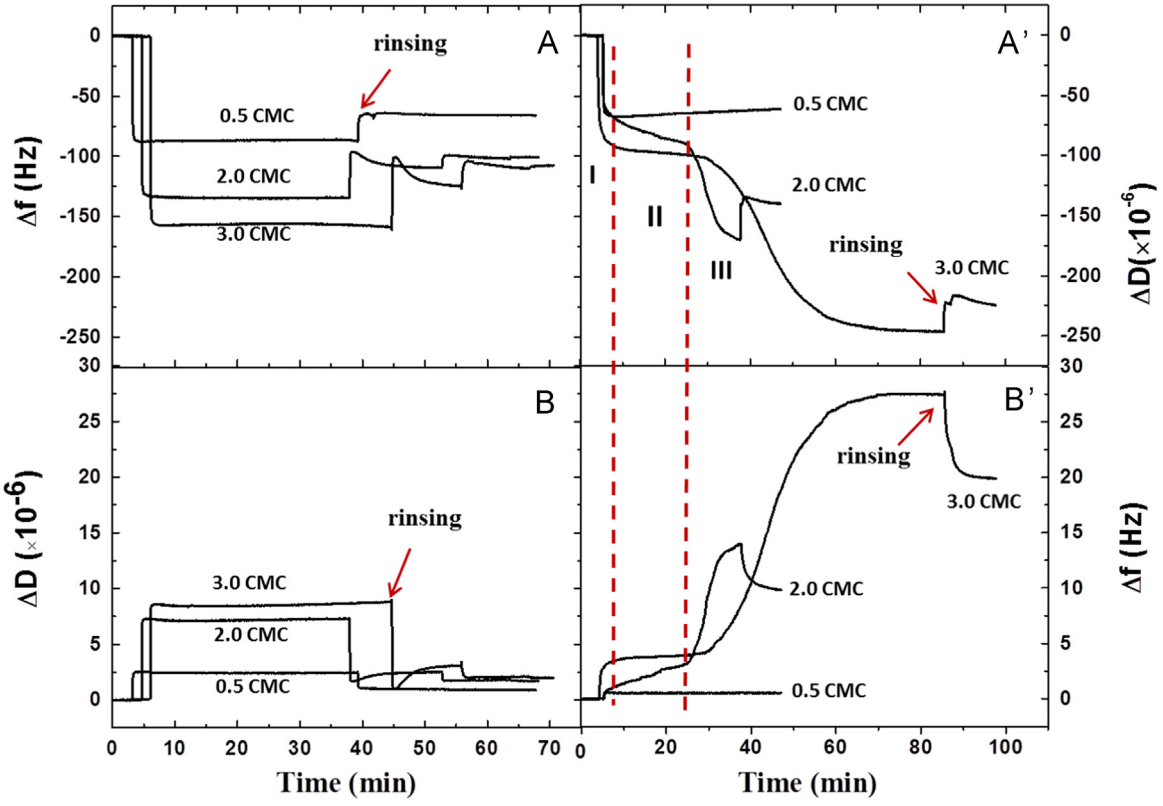

Fig. 1. Adsorption dynamics of P500 (a, b) and P100 (a′, b′) characterized using a quartz resonator with frequency (Δf) and dissipation (ΔD). The dashed lines indicate the three regions of the kinetic adsorption of P100 at 2.0 CMC.

change irrespective of whether the concentration is below or above the CMC. This behavior reveals that the equilibrium state is established after the initial fast adsorption process and that the adsorption dynamics mode is independent of the P500 concentration.

The adsorption dynamics of P100 are significantly distinct. As shown in Fig. 1a′ and b′, when the polymeric concentration is 0.5 CMC, the adsorption kinetics are similar to that of P500. In contrast, when the concentration is above the CMC, the adsorption dynamics of P100 exhibit three typical adsorption regimes, which correspond to the initial adsorption stage (regime I), the limited adsorption stage (regime II) and the re-adsorption stage (regime III). In particular, $-\Delta f$ and ΔD increase significantly in regime I, which suggests that the free chains adsorb quickly from the solution onto the surface. In regime II, $-\Delta f$ and ΔD change slowly. In regime III, P100 exhibits fast adsorption again. In other words, compared to the adsorption dynamics of P500, a deceleration and acceleration during the adsorption process occur for P100. The acceleration of adsorption has been observed previously in the grafting of polymer chains onto a surface (Penn et al., 2000; Liu et al., 2005).

To explore the mechanism for the distinct adsorption dynamics modes, Figs. 2 and 3 depict the typical simulation snapshots of the adsorption process for P100 and P500, respectively. In these simulations, the numbers of P100 and P500 copolymers are set at 200 to generate the concentrations beyond the CMC (unless otherwise specified, the concentration remains unchanged in the following discussion on the simulation results). Different polymer concentrations were tried including 20, 40, 60 and 80 P100/P500 polymer chains, and qualitatively same results were obtained. Three adsorption stages, namely the initial adsorption, limited adsorption and re-adsorption, can be clearly observed from the snapshots for P100. Specifically, from Fig. 2A to B, it is clear that copolymers near the hydrophobic surface are quickly adsorbed to the surface, which is in agreement with the experimental observations discussed above. Simultaneously, the copolymers in the bulk water aggregate and form micelles (see the middle area in Fig. 2B). Nolan et al. (1997) argued that PEO–PPO–PEO triblock copolymers of the same type formed micelles of relatively uniform size, and this is generally confirmed by our simulation. Furthermore, because the hydrophilic PEO block in P100 is relatively short, the hydrophobic PPO micelle cores are unstable. As a result, more and more free copolymer in solution is gradually incorporated into the small micelles to stabilize their structure. This leads to micelle growth (Zhang et al., 2001). This behavior is evident from the variation between Fig. 2B and C. Meanwhile, the remaining free chains diffuse into the vicinity of the surface and are finally adsorbed due to the strong attractive force between the PPO blocks. This process is diffusion-controlled and slow, and it corresponds to the limited adsorption stage observed experimentally.

From Fig. 2D–F, we found that the micelles are adsorbed to the polymer layer on the hydrophobic surface and finally melt and are adsorbed. This is because the hydrophilic shell around the micelle is too weak to stabilize the assembled structure, and the micelle can easily disaggregate because of the interactions from the

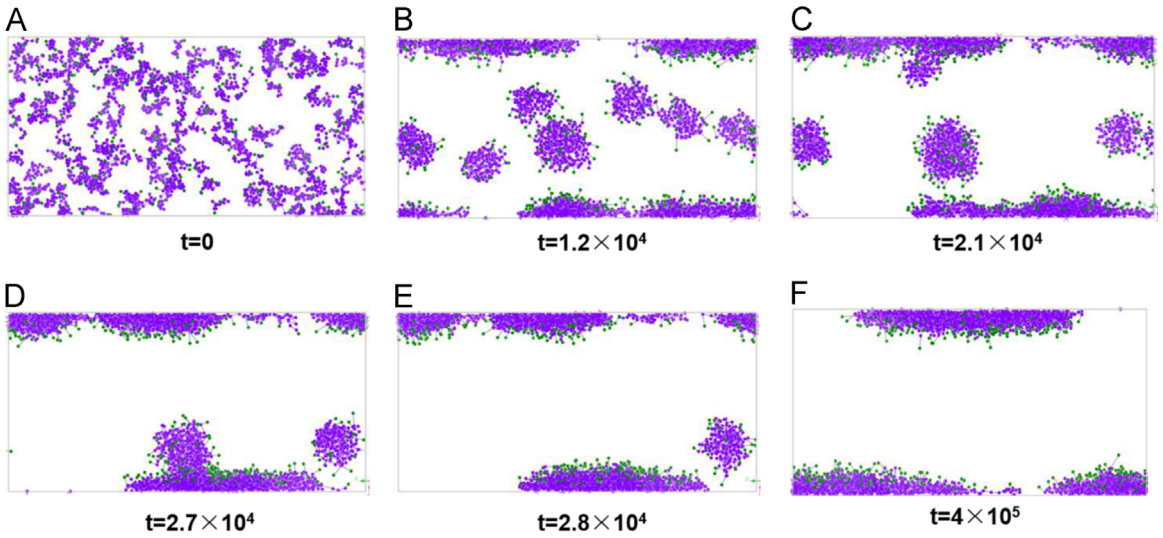

Fig. 2. Typical simulation snapshots during the adsorption process of P100. The PO bead is violet, and the EO bead is green. Water beads are omitted for simplicity. (A) Initial configuration. (B)–(E) Intermediate adsorption process. (F) Final equilibrium state of the system. (For interpretation of the references to color in this figure legend, the reader is referred to the web version of this article.)

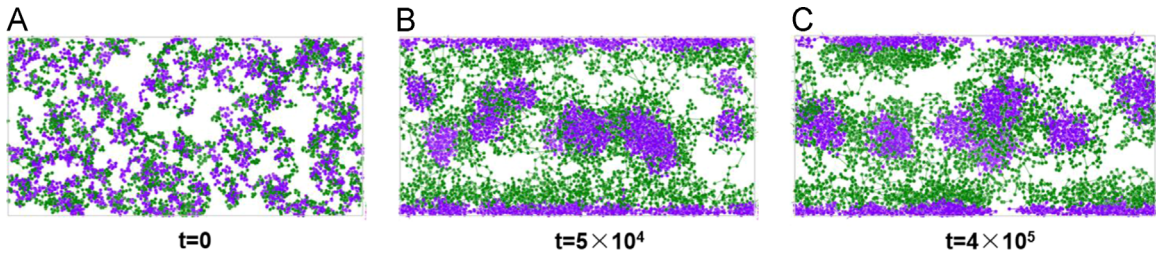

Fig. 3. Typical simulation snapshots during the adsorption process of P500. The PO bead is violet, and the EO bead is green. Water beads are not shown for simplicity. (A) Initial configuration. (B) Intermediate state of adsorption. (C) Final equilibrium state of the system. (For interpretation of the references to color in this figure legend, the reader is referred to the web version of this article.)

surface and existent adsorbed layer. This disaggregation leads to the final fast re-adsorption of P100. In this regime, the micelles resemble a reservoir to the feed polymer chains for the adsorption. The similar "feeding mechanism" was also observed by Srinivas et al. (2006) in a confined simulation system with aqueous surfactants.

Fig. 3 plots three typical snapshots during the adsorption process of P500. Similar to P100, the quick adsorption for P500 near two hydrophobic surfaces is also observed at the beginning. However, after this initial period, no further adsorption was found. The comparison of Fig. 3C and Fig. 2F reveals that the micelles composed of P500 are stable in solution and they contain a large hydrophilic corona and do not approach the surface or merge into the adsorbed polymer layer on the surface. Such resistance is likely due to the strong solvent-mediated repulsion between the hydrophilic PEO blocks. It is generally believed that PEO–PPO–PEO chains form a monolayer on the hydrophobic surface with the insoluble PPO blocks as the anchors and soluble PEO blocks as buoys (Brandani and Stroeve, 2003; Marques et al., 1988; Johner and Joanny, 1990; Brandani and Stroeve, 2003). For the adsorbed P500, all dangling hydrophilic PEO blocks stretch away from the hydrophobic surface into the solution, constituting a hydrophilic brush. When compared to P100, the brushes formed from the P500 polymer are more significant and palpable, as shown in Fig. 3C. The long hydrophilic brushes repel the micelles and thus hinder the further adsorption.

To quantify the adsorption dynamics, we calculated the number of copolymers adsorbed onto the surface at different simulation time for both P100 and P500 systems. The calculated amounts of copolymer as a function of simulation steps are shown in Fig. 4 (black lines with symbols). In our calculation, the copolymer is considered to be adsorbed once it is located within a certain distance from the hydrophobic surface of $4.5r_c$ for P100 and $4.0r_c$ for P500. These distances are determined by identifying the average heights of the resultant semi-micelles on the surface. The final results were obtained by taking average over 20 different simulation trials. For simplicity only the error bars for the adsorption curve of P100 is displayed. As shown in Fig. 4, the amount of adsorbed P500 remains almost unchanged after the initial fast adsorption. In contrast, the adsorption of P100 can be divided into three regimes. For direct comparison with experimental observation, the adsorption curve of P100 at 2.0 CMC (ΔD from Fig. 1) is also added. This comparison exhibits a linear correspondence

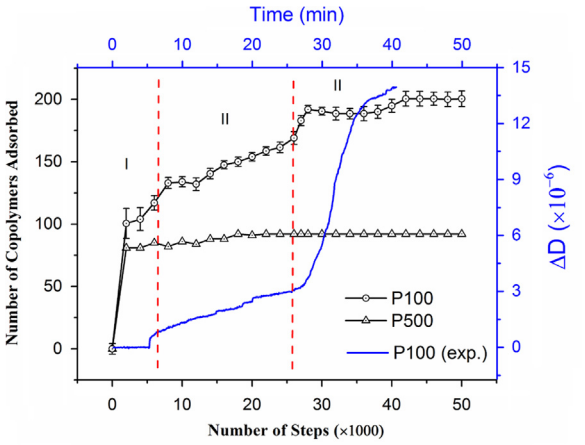

Fig. 4. The calculated number of copolymers adsorbed onto the surface as a function of simulation steps (lines with symbols). For comparison, the experimental curve of ΔD for P100 at 2.0 CMC is present (blue line). The typical three regimes observed for P100 are marked as I, II and III. Lines are drawn to guide the eye. (For interpretation of the references to color in this figure legend, the reader is referred to the web version of this article.)

between the simulation process and the experimental one, i.e., the time points for three adsorption regimes in both simulation and experiment are linearly related. Note that the scale involved in this linear relation generally depends on both the system size of theoretical model and the polymer concentration in the system, and it is meaningless to discuss this value upon a designated set of simulation results. The slope of the curve represents the adsorption speed. In regime I, the slope is very large, particularly within the first few hundred steps. The slope then decreases in the second regime before increasing again in the last regime. It should be noted that the slope finally becomes zero in regime III due to the equilibration of the system. In simulation the slope in regime III quickly becomes zero likely resulting from the very limited system size. The simulation results are overall consistent with the experimental observations, which confirms the validity of the adsorption details as discussed in Figs. 2 and 3.

The combination of experimental and simulation results provide further insight into the adsorption dynamics as a whole to give a clearer picture. When the concentration is below the CMC, the adsorption dynamics are trivial for both P500 and P100 and no micelles are formed. The polymer chains are adsorbed directly from the solution to the hydrophobic surface until the balance between adsorption and desorption is achieved. When the concentration exceeds the CMC, P500 and P100 present distinct adsorption modes. For P500, the free polymer chains in the bulk solution aggregate and form micelles. The free chains in the vicinity of the hydrophobic surface are adsorbed, which exhibits fast adsorption as observed experimentally, and the micelles are then repelled from the adsorbed polymer layer on the surface and remain in solution. Therefore, no further adsorption occurs. For P100, three adsorption regimes were observed. In addition to the fast adsorption that is also observed for P500, two additional adsorption regimes occurred that are associated with the weak stability of the formed micelles. After the fast adsorption, the free polymer chains in solution, which are participating in an aggregation and disaggregation equilibrium with the micelles, diffuse to the vicinity of the surface and are adsorbed. This process is diffusion-controlled and thus appears as a slow adsorption. The final fast re-adsorption occurs when the micelles near the surface resolve and supply free polymer chains.

The adsorption dynamics, which are determined from the hydrophilic PEO block length, can be disrupted through competitive interactions. When the PEO block length is short, the attraction between the hydrophobic PPO blocks dominates, and this attraction results in the three-regime adsorption of polymer onto the surface. In contrast, when the PEO block length is long, the repulsion between the hydrophilic PEO blocks dominates, and thus, only a few polymer chains are adsorbed.

4.2. Adsorbed structures of P500 and P100

The morphologies of various types of triblock copolymers adsorbed on different substrates have been extensively investigated (Shi et al., 2004; Li et al., 2012; Liu et al., 2011). Here, we have explored the adsorbed structures of P500 and P100 at various concentrations. Understanding the adsorption structure is very helpful for surface modification and material fabrication.

To explore the structural changes in the adsorbed polymer layer, the relationship between ΔD and Δf during the adsorption process at different polymeric concentrations was analyzed. The slope of the ΔD–Δf curve is related to the viscoelasticity of the polymeric layer on the surface. In other words, more curvature suggests more variation in the layer conformation. Fig. 5 plots the relationship between ΔD and Δf for P500 (a–c) and P100 (a′–c′). During the adsorption of P500, ΔD linearly increases with $-\Delta f$ regardless of rinsing. This behavior suggests that the adsorbed

layer is homogeneous. Regardless of the concentration, the linear relationship between ΔD and Δf is retained. This result indicates that the adsorbed layers form similar structures irrespective of the concentration of the P500 solution. However, as shown in Fig. 5b′ and c′, a clear curvature of the ΔD–Δf curve is observed for P100 when the concentration exceeds the CMC. This behavior implies that a two-layer structure is formed in the P100 system. In addition, we found that the threshold value of Δf, which corresponds to the cross-over point of the fold line and the red dashed line in Fig. 5b′ or c′, is nearly identical to the critical value of Δf at the same polymer concentration in Fig. 1a′ that divides regime II and regime III. This observation suggests two key points in the adsorption of P100 at concentrations above the CMC. First, although the adsorption speeds in regime I and regime II are distinct as discussed above, the resultant polymer structures on the surface appear to be the same. In other words, the types of adsorbates in both regimes appear similar. Because in regime I a fast adsorption of free chains from solution onto the surface takes place, we conclude hereafter that in regime II, the adsorbates are mainly the free polymer chains of P100. Second, the polymer structure in the outer layer is formed within the adsorption regime III predominantly, and the viscoelasticity differs from the inner layer. This indicates that the types of adsorbates in this adsorption regime are distinct or are in different states, viz., the adsorbates are at the least not composed predominantly of free chains as in the previous two regimes.

To explore the structure of the adsorbed polymer layer at different polymeric concentrations, Fig. 6 depicts the concentration dependence of Δf and ΔD for both P100 and P500. Here, Δf and ΔD are equilibrium values before rinsing. Δf is proportional to the mass of adsorbed polymer on the surface, and ΔD indicates the softness of the polymer layer. For P500, both Δf and ΔD increase linearly with concentration over the entire concentration range, and this indicates that the adsorbed layer presents similar compactness regardless of polymer concentration. However, for P100, $-\Delta f$ and ΔD exhibit a piecewise linear dependence with concentration. In particular, when the concentration is above the CMC, the slopes of both $-\Delta f$ and ΔD sharply increase, implying that more chains are adsorbed onto the surface and that the adsorbed layer is more compact than at concentrations below the CMC.

Similar results were also found using SPR analysis. As discussed above, the SPR response relates to the refractive index in the vicinity of the surface. Namely, both the adsorbed polymer layer and polymer solution near the interface contribute to the SPR response. Because the thickness of the polymer layer (~several nanometers, see below) is much less than the detection depth of the apparatus (~200 nm), the signal is dominated predominantly by the solution. As a result, SPR analysis does not reflect the adsorption dynamics. Nevertheless, ΔR reflects the concentration of the polymer near the sensor surface (Brandani and Stroeve, 2003). Fig. 7 plots ΔR for both polymer

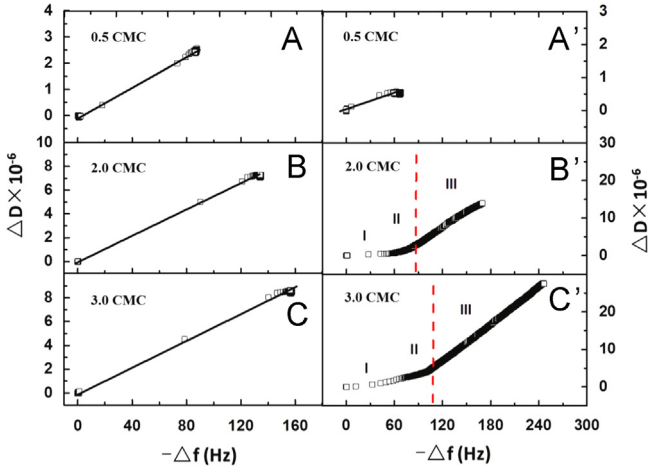

Fig. 5. The relationship between ΔD and Δf for P500 (a–c) and P100 (a′–c′). From top to bottom, the concentrations are 0.5 CMC (a, a′), 2.0 CMC (b, b′) and 3.0 CMC (c, c′), respectively.

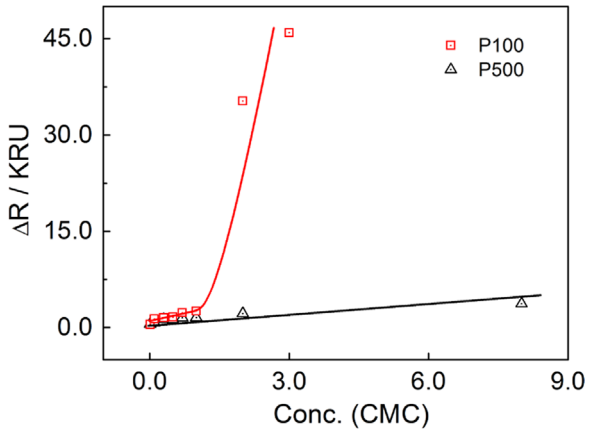

Fig. 7. SPR responses (ΔR) for P100 and P500 at various polymer concentrations in solution.

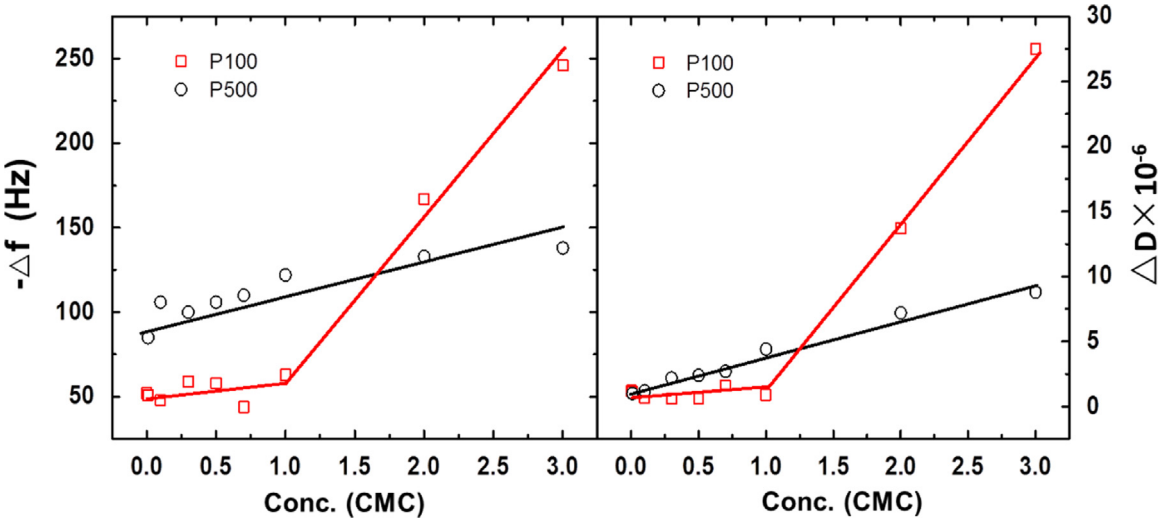

Fig. 6. Concentration dependence of the frequency (Δf) and dissipation (ΔD) for P100 (squared lines) and P500 (circled lines).

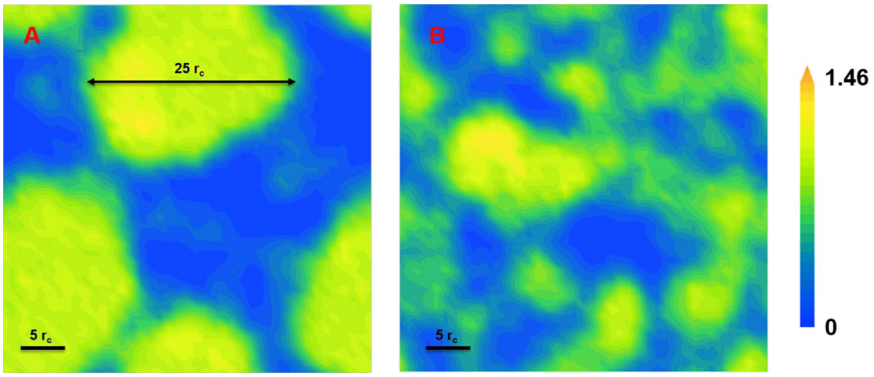

Fig. 8. Typical contour plots of the number density of PO beads on the hydrophobic surface ($z=0$ plane) for (A) P100 and (B) P500 at equilibrium.

solutions at different polymer concentrations. Again, ΔR is the equilibrium value before rinsing.

It should be noted that these curves are not directly comparable with each other because the polymers in both systems are different. However, the curve type for each system indicates the adsorption sensitivity with polymer concentration. For P500, the linear relationship between ΔR and concentration suggests that the adsorption mode is the same regardless of the concentration. For P100, ΔR gradually increases at concentrations below the CMC but sharply increases when the concentration exceeds the CMC. This suggests that the adsorption mode changes beyond the CMC. As the slope becomes larger after the concentration exceeds the CMC, we can deduce that a more compact structure is formed on the surface.

To explicitly understand the structure, the simulation results in the final equilibrium state were analyzed and compared to the morphology of the adsorbed polymers. This analysis not only serves as a validation by comparing with the empirical findings but also further explores the difference in the mechanism by which the triblock copolymer with different hydrophilic block lengths is adsorbed to the hydrophobic surface. Towards that end, the typical contour plots of the number density of PO beads on the hydrophobic surface ($z=0$ plane) for both P100 and P500 are shown in Fig. 8. For P100, a semi-micelle morphology is observed as shown in Fig. 8A. The lateral dimension of the semi-micelle is approximately 22.4 nm (equivalent to $25r_c$), and the vertical dimension is approximately 3.6 nm (equivalent to $4r_c$). These results are consistent with reported experimental data (30 nm laterally, and 1 nm vertically) (Brandani and Stroeve, 2003), although these experiments were conducted with P300 with relatively longer PEO blocks at lower concentrations (1 CMC). As shown in Fig. 8B the P500 polymers exhibit a different morphology compared to the adsorbed P100 polymers, and are more uniformly adsorbed onto the surface than the latter. This result confirms the macroscopic observation of homogeneous and smooth polymer at higher concentrations (10 CMC) (Brandani and Stroeve, 2003).

5. Conclusion

In the present study, the adsorption dynamics of two different types of symmetrical PEO–PPO–PEO triblock copolymers onto a hydrophobic solid surface are investigated using DPD simulations and in situ experimental techniques including Laser Light Scattering and QCM-D measurements. These triblock copolymers, i.e., P100 and P500, have the same middle hydrophobic PPO block and different hydrophilic PEO block lengths. By characterizing the physicochemical properties of the adsorbed polymer layer on the solid surface during the adsorption process, we have demonstrated that the adsorption dynamics of these triblock copolymers are determined not only by the polymer concentration but also by the PEO block length.

First, at low bulk concentrations (below the CMC), the adsorption dynamics of both types of copolymers are simple and similar, and only fast adsorption is observed. When the polymer concentration exceeds the CMC, the adsorption dynamics for P100 and P500 become distinct. While the adsorption for the copolymers with long PEO block lengths (i.e., P500) remains monotonous, P100 presents an interesting three-stage adsorption mode including an initial fast adsorption, a diffusion-controlled limited adsorption, and then a final fast re-adsorption due to the disaggregation of micelles in the vicinity of the liquid/solid interface. Second, the adsorbed polymer layer of P500 on the hydrophobic surface presents a homogeneous structure regardless of the concentration used, while a two-layer structure for adsorbed P100 is found when the polymer concentration exceeds the CMC. The inner layer is formed during the first two adsorption stages, and the outer layer is formed during the final adsorption stage. Third, the mechanism by which the block length determines the adsorption dynamics is explored by the complementary DPD simulation study from the perspective of molecular interactions. The adsorption dynamic behavior originates from the competitive solvent-mediated polymer–polymer interaction and the polymer–surface interaction. In particular, for copolymers with a relatively short hydrophilic block such as P100, the repulsion between the hydrophilic blocks is weak, which is overcome by the stronger attraction between the hydrophobic blocks when more and more polymer is adsorbed onto the surface. This competition results in the three-regime adsorption of polymer onto the surface. In contrast, for the P500 system, the repulsion between the hydrophilic PEO blocks dominates, and this hinders further adsorption. Therefore, the adsorption mode of P500 is monotonous.

The present experimental–numerical study provides a mechanistic interpretation on the adsorption dynamics of copolymers onto a liquid/solid interface and casts helpful insight into the dynamic control process of surface modification and material fabrication.

Acknowledgments

This work is supported by the National Basic Research Program of China (2014CB748500), the National Natural Science Foundation of China (Nos. 21306049, 91434110 and 51403062), the 111 Project of the Ministry of Education of China (No. B08021), the Open Project of State Key Laboratory of Chemical Engineering of China (SKL-ChE-13C04), and the Innovation Program of Shanghai Municipal Education Commission (15ZZ029, 15ZZ030). SZ also

acknowledges the support of the Shanghai Science and Technology Committee Rising-Star Program (No. 14QA1401300).

References

Napper, D.H., 1983. Polymeric Stabilization of Colloidal Dispersions. Academic Press, London.

Chakraborty, A.K., Golumbfskie, A.J., 2001. Polymer adsorption-driven self-assembly of nanostructures. Annu. Rev. Phys. Chem. 52, 537–573.

Frisch, H.L., Simha, R., Eirich, F.R., 1953. Statistical mechanics of polymer adsorption. J. Chem. Phys. 21 (2), 365–366.

Silberberg, A., 1962. Adsorption of flexible macromolecules. 1. Isolated macromolecule at a plane interface. J. Phys. Chem. 66 (10), 1872–1883.

Scheutjens, J., Fleer, G.J., 1979. Statistical-theory of the adsorption of interacting chain molecules. 1. Partition-function, segment density distribution, and adsorption-isotherms. J. Phys. Chem. 83 (12), 1619–1635.

Watts, T.H., Brian, A.A., Kappler, J.W., Marrack, P., McConnell, H.M., 1984. Antigen presentation by supported planar membranes containing affinity-purified I-Ad. In: Proceedings of National Academy of Sciences of the United States of America-Biological Sciences. 81(23), pp. 7564–7568.

Munch, M.R., Gast, A.P., 1988. Block copolymers at interfaces. 2. Surface-adsorption. Macromolecules 21 (5), 1366–1372.

Zhu, B.Y., Gu, T.R., 1991. Surfactant adsorption at solid–liquid interfaces. Adv. Colloid Interface Sci. 37 (1–2), 1–32.

Wang, Y.M., Mattice, W.L., 1994. Adsorption of homopolymers on a solid-surface – a comparison between Monte-Carlo simulation and the Scheutjens-Fleer mean-field lattice theory. Langmuir 10 (7), 2281–2288.

Zhan, Y.J., Mattice, W.L., 1994. Self-assembly and adsorption of diblock copolymers from selective solvents. 1. Self-assembly. Macromolecules 27 (3), 677–682.

Amiel, C., Sikka, M., Schneider, J.W., Tsao, Y.H., Tirrell, M., Mays, J.W., 1995. Adsorption of hydrophilic-hydrophobic block-copolymers on silica from aqueous-solutions. Macromolecules 28 (9), 3125–3134.

Misra, D.N., 1996. Adsorption of polyacrylic acids and their sodium salts on hydroxyapatite: effect of relative molar mass. J. Colloid Interface Sci. 181 (1), 289–296.

Huang, N.P., Csucs, G., Emoto, K., Nagasaki, Y., Kataoka, K., Textor, M., Spencer, N.D., 2002. Covalent attachment of novel poly(ethylene glycol)–Poly(DL-lactic acid) copolymeric micelles to TiO_2 surfaces. Langmuir 18 (1), 252–258.

Brandani, P., Stroeve, P., 2003. Adsorption and desorption of PEO–PPO–PEO triblock copolymers on a self-assembled hydrophobic surface. Macromolecules 36 (25), 9492–9501.

Li, Y., Liu, H., Song, J., Rojas, O.J., Hinestroza, J.P., 2011. Adsorption and association of a symmetric PEO–PPO–PEO triblock copolymer on polypropylene, polyethylene, and cellulose surfaces. ACS Appl. Mater. Interfaces 3 (7), 2349–2357.

Kamerlin, S.C.L., Vicatos, S., Dryga, A., Warshel, A., 2011. Coarse-grained (multiscale) simulations in studies of biophysical and chemical systems. Annu. Rev. Phys. Chem. 62 (1), 41–64.

Marques, C., Joanny, J.F., Leibler, L., 1988. Adsorption of block copolymers in selective solvents. Macromolecules 21 (4), 1051–1059.

Johner, A., Joanny, J.F., 1990. Block copolymer adsorption in a selective solvent – a kinetic-study. Macromolecules 23 (26), 5299–5311.

Munch, M.R., Gast, A.P., 1990. Kinetics of block copolymer adsorption on dielectric surfaces from a selective solvent. Macromolecules 23 (8), 2313–2320.

Tiberg, F., Malmsten, M., Linse, P., Lindman, B., 1991. Kinetic and equilibrium aspects of block copolymer adsorption. Langmuir 7 (11), 2723–2730.

Alexandridis, P., Holzwarth, J.F., Hatton, T.A., 1994. Micellization of poly(ethylene oxide)–poly(propylene oxide)–poly(ethylene oxide) triblock copolymers in aqueous-solutions-thermodynamics of copolymer association. Macromolecules 27 (9), 2414–2425.

Eskilsson, K., Tiberg, F., 1997. Equilibrium and kinetic properties of triblock copolymers at hydrophobic surfaces. Macromolecules 30 (20), 6323–6332.

Green, R.J., Tasker, S., Davies, J., Davies, M.C., Roberts, C.J., Tendler, S.J.B., 1997. Adsorption of PEO–PPO–PEO triblock copolymers at the solid/liquid interface: a surface plasmon resonance study. Langmuir 13 (24), 6510–6515.

Emoto, K., Nagasaki, Y., Kataoka, K., 1999. Coating of surfaces with stabilized reactive micelles from poly(ethylene glycol)-poly(DL-lactic acid) block copolymer. Langmuir 15 (16), 5212–5218.

Chen, T., Guo, L., Liu, H., Hu, Y., 2003. Studies of adsorption of diblock copolymers from non-selective solvent by Scheutjens-Fleer theory and Monte Carlo simulation, 1. Macromol. Theory Simul. 12 (2–3), 153–162.

Chen, T., Liu, H., Hu, Y., 2001. Monte Carlo simulation for the adsorption of diblock copolymers. I. In nonselective solvent. J. Chem. Phys. 114 (13), 5937.

Guo, L., Chen, T., Liu, H., Hu, Y., 2003. Studies of adsorption of diblock copolymers from non-selective solvent by Scheutjens-Fleer theory and Monte Carlo simulation, 2. Macromol. Theory Simul. 12 (2–3), 163–173.

Tong, C., 2014. Numerical study of weak polybase brushes grafted on neutral or charged spherical surface by the self-consistent field theory. Langmuir 30 (50), 15301–15308.

Lian, C., Chen, X., Zhao, S., Lv, W., Han, X., Wang, H., Liu, H., 2014. Substrate effect on the phase behavior of polymer brushes with lattice density functional theory. Macromol. Theory Simul. 23 (9), 575–582.

Lian, C., Wang, L., Chen, X., Han, X., Zhao, S., Liu, H., Hu, Y., 2014. Modeling swelling behavior of thermoresponsive polymer brush with lattice density functional theory. Langmuir 30 (14), 4040–4048.

BASF (China) Co. LTD.,: No. 300 Jiangxinsha Road, Pudong New District, Shanghai, China.

SINOPHARM, China National Pharmaceutical Group Corporation (SINOPHARM): No. 20 Zhichun Road, Haidian District, Beijing, China.

Creager, S.E., Clarke, J., 1994. Contact-angle titrations of mixed omega-mercaptoalkanoic acid alkanethiol monolayers on gold-reactive vs non-reactive spreading, and chain-length effects on surface pKa values. Langmuir 10 (10), 3675–3683.

Langen, A.L.V., ALV-Laser Vertriebsgesellschaft m-b.H.: Siemensstrasse 4, D-63225 Langen/Hessen, Germany.

Rodahl, M., Hook, F., Krozer, A., Brzezinski, P., Kasemo, B., 1995. Quartz-crystal microbalance setup for frequency and Q-factor measurements in gaseous and liquid environments. Rev. Sci. Instrum. 66 (7), 3924–3930.

Sauerbrey, G., 1959. Verwendung Von Schwingquarzen Zur Wagung Dunner Schichten Und Zur Mikrowagung. Z. Fur Phys. 155 (2), 206–222.

Zheng, B., Bi, J.-h, Dong, H.-z, Zhu, J.-m., Liang, H.-j., 2014. Adsorption of microcystin onto polymer covered gold chips by quartz crystal microbalance-dissipation detection. Chin. J. Chem. Phys. 27 (6), 739–744.

Stockbridge, C.D., 1966. Katz, M.J. (Ed.), vacuum microbalance techniques. Plenum Press, New York.

Kanazawa, K.K., Gordon, J.G., 1985. Frequency of a quartz microbalance in contact with liquid. Anal. Chem. 57 (8), 1770–1771.

Rodahl, M., Kasemo, B., 1996. On the measurement of thin liquid overlayers with the quartz-crystal microbalance. Sens. Actuators A – Phys. 54 (1–3), 448–456.

Lucklum, R., Hauptmann, P., 2003. Transduction mechanism of acoustic-wave based chemical and biochemical sensors. Meas. Sci. Technol. 14 (11), 1854–1864.

BIAcore X., G.E. Healthcare: Björkgatan 30, Box 605, 75125 Uppsala, Sweden.

Sjolander, S., Urbaniczky, C., 1991. Integrated fluid handling-system for biomolecular interaction analysis. Anal. Chem. 63 (20), 2338–2345.

Pockrand, I., 1978. Surface plasma-oscillations at silver surfaces with thin transparent and absorbing coatings. Surf. Sci. 72 (3), 577–588.

Knoll, W., 1998. Interfaces and thin films as seen by bound electromagnetic waves. Annu. Rev. Phys. Chem. 49, 569–638.

Groot, R.D., Warren, P.B., 1997. Dissipative particle dynamics: bridging the gap between atomistic and mesoscopic simulation. J. Chem. Phys. 107 (11), 4423.

Keaveny, E.E., Pivkin, I.V., Maxey, M., Em Karniadakis, G., 2005. A comparative study between dissipative particle dynamics and molecular dynamics for simple- and complex-geometry flows. J. Chem. Phys. 123 (10), 104107.

Feng, J., Liu, H., Hu, Y., 2007. Micro-phase separation of diblock copolymer in a nanosphere: dissipative particle dynamics approach. Fluid Phase Equilib. 261 (1), 50–57.

Feng, J., Liu, H., Hu, Y., 2006. Mesophase separation of diblock copolymer confined in a cylindrical tube studied by dissipative particle dynamics. Macromol. Theory Simul. 15 (9), 674–685.

Hoogerbrugge, P., Koelman, J., 1992. Simulating microscopic hydrodynamic phenomena with dissipative particle dynamics. Eur. Lett. 19 (3), 155.

Espanol, P., Warren, P., 1995. Statistical mechanics of dissipative particle dynamics. Eur. Lett. 30 (4), 191.

Chen, S., Hu, G.-H., Guo, C., Liu, H.-Z., 2007. Experimental study and dissipative particle dynamics simulation of the formation and stabilization of gold nanoparticles in PEO–PPO–PEO block copolymer micelles. Chem. Eng. Sci. 62 (18), 5251–5256.

Groot, R.D., Rabone, K.L., 2001. Mesoscopic simulation of cell membrane damage, morphology change and rupture by nonionic surfactants. Biophys. J. 81 (2), 725–736.

Bandyopadhyay, S., Shelley, J.C., Tarek, M., Moore, P.B., Klein, M.L., 1998. Surfactant aggregation at a hydrophobic surface. J. Phys. Chem. B 102 (33), 6318–6322.

Lee, S.H., Rossky, P.J., 1994. A comparison of the structure and dynamics of liquid water at hydrophobic and hydrophilic surfaces – a molecular dynamics simulation study. J. Chem. Phys. 100 (4), 3334–3345.

Srinivas, G., Nielsen, S.O., Moore, P.B., Klein, M.L., 2006. Molecular dynamics simulations of surfactant self-organization at a solid–liquid interface. J. Am. Chem. Soc. 128 (3), 848–853.

Shi, K., Lian, C., Bai, Z., Zhao, S., Liu, H., 2014. Dissipative particle dynamics study of the water/benzene/caprolactam system in the absence or presence of non-ionic surfactants. Chem. Eng. Sci. 122, 185–196.

Accelrys, Materials Studio. Accelrys Software Inc.

Groot, R.D., Warren, P.B., 1997. Dissipative particle dynamics: bridging the gap between atomistic and mesoscopic simulation. J. Chem. Phys. 107 (11), 4423–4435.

Sun, L., Peng, C., Liu, H., Hu, Y., 2007. Influence of polymer structure on adsorption behavior at solid–liquid interface by Monte Carlo simulation. Mol. Simul. 33 (12), 989–997.

Peng, C., Li, J., Liu, H., Hu, Y., 2005. Monte Carlo Simulation for the adsorption of symmetric triblock copolymers II. Adsorption layer information. Eur. Polym. J. 41 (3), 637–644.

Penn, L.S., Hunter, T.F., Lee, Y., Quirk, R.P., 2000. Grafting rates of amine-functionalized polystyrenes onto epoxidized silica surfaces. Macromolecules 33 (4), 1105–1107.

Liu, G.M., Cheng, H., Yan, L.F., Zhang, G.Z., 2005. Study of the kinetics of the pancake-to-brush transition of poly(N-isopropylacrylamide) chains. J. Phys. Chem. B 109 (47), 22603–22607.

Nolan, S.L., Phillips, R.J., Cotts, P.M., Dungan, S.R., 1997. Light scattering study on the effect of polymer composition on the structural properties of PEO–PPO–PEO micelles. J. Colloid Interface Sci. 191 (2), 291–302.
Zhang, G.Z., Niu, A.Z., Peng, S.F., Jiang, M., Tu, Y.F., Li, M., Wu, C., 2001. Formation of novel polymeric nanoparticles. Acc. Chem. Res. 34 (3), 249–256.
Brandani, P., Stroeve, P., 2003. Adsorption and desorption of $PEO_{61}PPO_{61}PEO$ triblock copolymers on a self-assembled hydrophobic surface. Macromolecules 36 (25), 9492–9501.
Shi, H., Zhang, S., Steitz, R., Chen, J., Uredat, S., Findenegg, G.H., 2004. Surface coatings of PEO–PPO–PEO block copolymers on native and polystyrene-coated silicon wafers. Colloids Surf. A Physicochem. Eng. Asp. 246 (1–3), 81–89.
Li, Y., Rojas, O.J., Hinestroza, J.P., 2012. Boundary lubrication of PEO–PPO–PEO triblock copolymer physisorbed on polypropylene, polyethylene, and cellulose surfaces. Ind. Eng. Chem. Res. **51** (7), 2931–2940.
Liu, H., Li, Y., Krause, W.E., Pasquinelli, M.A., Rojas, O.J., 2011. Mesoscopic simulations of the phase behavior of aqueous EO_{19} PO_{29} EO_{19} solutions confined and sheared by hydrophobic and hydrophilic surfaces. ACS Appl. Mater. Interfaces 4 (1), 87–95.